Magnetism and thermodynamics of spin-($\frac{1}{2}$,1) decorated Heisenberg chain with spin-1 pendants

Shou-Shu Gong, Wei Li, Yang Zhao, and Gang Su*

College of Physical Sciences, Graduate University of Chinese Academy of Sciences, P.O. Box 4588, Beijing 100049, People's Republic of China

(Received 15 March 2010; revised manuscript received 24 May 2010; published 21 June 2010)

The magnetic and thermodynamic properties of a ferrimagnetic decorated spin-($\frac{1}{2}$,1) Heisenberg chain with spin-1 pendant spins are investigated for three cases: (A) $J_1, J_2 > 0$; (B) $J_1 > 0$ and $J_2 < 0$; and (C) $J_1 < 0$ and $J_2 > 0$, where J_1 and J_2 are the exchange couplings between spins in the chain and along the rung, respectively. The low-lying and magnetic properties are explored jointly by the real-space renormalization group, spin wave, and density-matrix renormalization-group methods, while the transfer-matrix renormalization-group method is invoked to study the thermodynamics. It is found that the magnon spectra consist of a gapless and two gapped branches. Two branches in case (C) have intersections. The coupling dependence of low-energy gaps are analyzed. In a magnetic field, a $m=\frac{3}{2}$ (m is the magnetization per unit cell) plateau is observed for case (A), while two plateaux at $m=\frac{1}{2}$ and $\frac{3}{2}$ are observed for cases (B) and (C). Between the two plateaux in cases (B) and (C), the sublattice magnetizations for the spins coupled by ferromagnetic interactions have decreasing regions with increasing the magnetic field. At finite temperature, the zero-field susceptibility temperature product χT and specific heat exhibit distinct exotic features with varying the couplings and temperature for different cases. χT is found to converge as $T \to 0$, which is different from the divergent behavior in the spin-($\frac{1}{2}$,1) mixed-spin chain without pendants. The observed thermodynamic behaviors are also discussed with the help of their low-lying excitations.

DOI: 10.1103/PhysRevB.81.214431 PACS number(s): 75.10.Jm, 75.40.Cx, 75.40.Mg, 75.50.Gg

I. INTRODUCTION

In recent years, one-dimensional (1D) quantum ferrimagnets with two kinds of antiferromagnetically exchange-coupled centers have attracted much attention due to their exotic properties. The large families of compounds ACu(pba)$(H_2O)_3 \cdot nH_2O$ and ACu(pbaOH)$(H_2O)_3 \cdot nH_2O$, where A=Mn,Fe,Co,Ni,Zn, pba=1,3-propylenebis, and pbaOH=2-hydroxy-1,3-propylenebis, have been extensively explored in chemistry,[1] which are good realizations of the mixed-spin chains. These compounds exhibit typically the 1D ferrimagnetic (FI) behavior of χT (χ is the magnetic susceptibility and T is the temperature) that shows a rounded minimum with temperature.[1]

As a simple model to describe the mixed-spin chains, the antiferromagnetically coupled spin-($\frac{1}{2}$,1) Heisenberg chain have also been extensively studied by various methods, such as the spin-wave theory,[2,3] Schwinger boson mean field,[4] density-matrix renormalization group (DMRG),[2] quantum Monte Carlo,[5] and so on.[6–8] It has been found that its ground state has a spontaneous magnetization at $m=\frac{1}{2}$ (m is the magnetization per unit cell) that is consistent with the Lieb-Mattis theorem,[9] and the system has a FI long-range order. The one-magnon excitation spectra consist of a gapless ferromagnetic (FM) branch from S_G to S_G-1 (S_G is the good quantum number of total spin in z component in the ground state) and a gapped antiferromagnetic (AFM) branch from S_G to S_G+1.[10] This magnon gap was numerically found to be $1.759J$ (J is the exchange coupling).[2] In a magnetic field, the system exhibits a magnetization plateau at $m=\frac{1}{2}$ with the width of $1.759J$, corresponding to the gap of the AFM magnon branch.[11] Different from the $S=1$ Haldane chain, in this mixed-spin chain the spin gap ($1.2795J$) from the ground state to the lowest state in the subspace of S_G+1 is less than the magnon gap ($1.759J$) and thus is not a magnonlike excitation.[2] The thermodynamic properties in the coexistence of the AFM and FM excitations[5,12] and in the critical phase under a magnetic field[7,13] have also been investigated.

Recently, another interesting family of cyanide-bridged coordination compounds with pendant magnetic ions are synthesized in experiment.[14,15] One of them is the cyanide-bridged Ni(II)-Fe(III) complex with an unusual building block $[Fe(1\text{-}CH_3im)(CN)_5]^{2-}$,[16] which can be treated as the 1D structure as shown schematically in Fig. 1 owing to the weak interchain interactions, where the Ni(II) (S_i and σ_i) and Fe(III) (τ_i) ions have spin 1 and $\frac{1}{2}$, respectively. This compound realizes a decorated spin-($\frac{1}{2}$,1) mixed-spin chain with spin-1 pendant spins. Although the intrachain couplings $J_1 < 0$ and $J_2 < 0$ are both FM interactions in the present compound, it is noticed that any other couplings (i.e., $J_1, J_2 > 0$, $J_1 > 0$ and $J_2 < 0$, and $J_1 < 0$ and $J_2 > 0$) would give rise to ferrimagnets, making the realization of such a FI structure more accessible to the experiment. This family of mixed-spin chains with pendant spins provides a scheme to study the 1D quantum ferrimagnetism, which may have exotic properties. Although the influences of pendant spins on magnetism have been discussed in some antiferromagnets,[17] the studies on such ferrimagnets are still rare till now.

In this paper, we shall explore the physical properties of this ferrimagnetic structure, and compare with the spin-($\frac{1}{2}$,1)

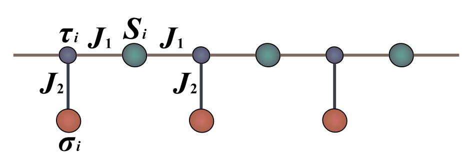

FIG. 1. (Color online) Sketch of the spin-(τ,S) decorated Heisenberg chain with spin-σ pendant spins.

mixed-spin chain without pendants. The low-lying, magnetic and thermodynamic properties of the spin-$(\frac{1}{2},1)$ decorated Heisenberg chain with spin-1 pendant spins for three cases: (A) $J_1,J_2>0$; (B) $J_1>0$ and $J_2<0$; and (C) $J_1<0$ and $J_2>0$ will be studied using various techniques. It is unveiled that due to the pendant spins, the ferrimagnets exhibit rather distinct magnetic and thermodynamic behaviors from those of the spin-$(\frac{1}{2},1)$ mixed-spin chain. The three cases with different couplings are uncovered to have their own features, which are expected to observe in experiments. The exotic properties of this system will also shed light on further understandings of quantum ferrimagnetism.

This paper is organized as follows. In Sec. II, the model Hamiltonian is introduced. In Sec. III, the low-energy effective Hamiltonians in both strong and weak couplings are analyzed utilizing the real-space RG (RSRG) method. The low-lying excitations and magnetic properties are investigated by the linear spin-wave (LSW) theory and DMRG in Sec. IV. In Sec. V, we shall study the zero-field thermodynamics by means of the transfer-matrix RG (TMRG). Finally, a summary and discussion will be given in Sec. VI.

II. MODEL HAMILTONIAN

The Hamiltonian of the spin-$(\frac{1}{2},1)$ decorated Heisenberg chain with spin-1 pendant spins in a magnetic field can be written as

$$H=\sum_{i=1}^{N}(J_1\vec{\tau}_i\cdot\vec{S}_i+J_1\vec{S}_i\cdot\vec{\tau}_{i+1}+J_2\vec{\tau}_i\cdot\vec{\sigma}_i)-h\sum_{i=1}^{N}(\tau_i^z+S_i^z+\sigma_i^z), \tag{1}$$

where $\vec{\sigma}_i$ is the $\sigma=1$ pendant spin, $\vec{\tau}_i$ and $\vec{S}_i$ are the spins in the chain with $\tau=\frac{1}{2}$ and $S=1$, respectively, $J_{1,2}>0$ (<0) denote the AFM (FM) couplings, and h is the magnetic field. Throughout the context, we take J_1 as an energy scale and $g\mu_B=1$. The schematic representation of the model is shown in Fig. 1.

Analogous to the spin-$(\frac{1}{2},1)$ mixed-spin chain without pendants, the system with Hamiltonian (1) has a spontaneous magnetization in the absence of magnetic field according to the Lieb-Mattis theorem.[9] In case (A) $(J_{1,2}>0)$ the spontaneous magnetization per unit cell is $m=\frac{3}{2}$ while in both cases (B) $(J_1>0,J_2<0)$ and (C) $(J_1<0,J_2>0)$ it is spontaneously magnetized at $m=\frac{1}{2}$. The Goldstone theorem[18] allows gapless excitations in these cases owing to the spontaneous breaking of the SU(2) symmetry.

III. REAL-SPACE RENORMALIZATION-GROUP ANALYSIS

In this section, the low-energy effective Hamiltonians of the three cases in both strong- and weak-coupling limits are derived utilizing the RSRG.[19] In the RSRG procedure, the Hamiltonian is divided into intrablock (H^B) and interblock (H^{BB}) parts. By diagonalizing H^B, a number of low-energy states are kept to project the full Hamiltonian into the renormalized Hilbert space. Although RSRG cannot give the results as accurate as the numerical approaches, it can give a good qualitative description for low-energy properties.

A. $J_1>0$ and $J_2>0$

Let us first consider the strong-coupling limit $(J_2\gg J_1)$. Since the interaction between τ_i and σ_i is strong, each rung can be considered as the isolated block in the first step of RG. Each block consists of two multiplets whose total spins are 1/2 and 3/2 with energies $-J_2$ and $J_2/2$, respectively. The spin-$\frac{1}{2}$ doublets are kept as the basis to construct the embedding operator T to project the full Hamiltonian onto the truncated Hilbert space. The effective Hamiltonian can be obtained as

$$\tilde{H}_{\rm A}^{\rm strong,1}=-NJ_2-\frac{1}{3}J_1\sum_{i=1}^{N}(\vec{S}_i'\cdot\vec{S}_i+\vec{S}_i\cdot\vec{S}_{i+1}'), \tag{2}$$

where $S_i'=1/2$ is the renormalized spin truncated from the rung block. Hamiltonian (2) describes a spin-$(\frac{1}{2},1)$ mixed-spin chain with a renormalized FM coupling $-\frac{1}{3}J_1$. In the next step of RG procedure, Hamiltonian (2) is further projected onto a $S''=3/2$ FM Heisenberg chain,

$$\tilde{H}_{\rm A}^{\rm strong,2}=-\left(J_2+\frac{J_1}{6}\right)N-\frac{2}{27}J_1\sum_{i=1}^{N}\vec{S}_i''\cdot\vec{S}_{i+1}''. \tag{3}$$

The magnon excitations in this FM Hamiltonian correspond to the magnons from S_G to S_G-1 in the original system, which are hence expected to be gapless with a quadratic dispersion in low energies. The RG can also give the sublattice magnetization $m_{\rm S}=1$, $m_\tau=-\frac{1}{6}$, and $m_\sigma=\frac{2}{3}$. The sum of them gives $\frac{3}{2}$, recovering the spontaneous magnetization of the original system.

In the weak-coupling limit $(J_2\ll J_1)$, the spins $\vec{\tau}_i$ and $\vec{S}_i$ are taken as a block, and the doublets with spin 1/2 are kept to truncate the block Hilbert space. The effective Hamiltonian is

$$\tilde{H}_{\rm A}^{\rm weak,1}=-NJ_1-\sum_{i=1}^{N}\left(\frac{4}{9}J_1\vec{S}_i'\cdot\vec{S}_{i+1}'+\frac{1}{3}J_2\vec{S}_i'\cdot\vec{\sigma}_i\right), \tag{4}$$

where $S_i'=1/2$ is the renormalized block spin. The Hamiltonian is mapped onto a spin-1/2 FM Heisenberg chain with $\sigma=1$ pendants coupled by the renormalized FM interaction $-\frac{1}{3}J_2$. The spin-wave analysis unveils that it has a gapless FM excitation with the dispersion

$$\omega_k\sim\frac{2}{27}J_1k^2 \tag{5}$$

for $k\to0$, which corresponds to the magnon excitation from S_G to S_G-1 of the original system. The sublattice magnetization is obtained as $m_{\rm S}=\frac{2}{3}$, $m_\tau=-\frac{1}{6}$, and $m_\sigma=1$, and the sum of them is also $\frac{3}{2}$.

From Eqs. (2) and (5) it can be seen that in the two coupling limits, the low-energy behaviors of the gapless branch are both dominated by J_1. Besides, $m_{\rm S}$ and m_σ exchange their values in the two limits, and m_τ is unchanged, implying a possible crossing of m_τ in the intermediate region of J_2/J_1, which would be confirmed by the DMRG results in the next section.

B. $J_1>0$ and $J_2<0$

In the strong-coupling limit ($|J_2|\gg J_1$), owing to the strong FM J_2, the low-energy multiplets with total spin 3/2 are kept to project the Hamiltonian in the first step of RG. The effective Hamiltonian is obtained as

$$\tilde{H}_{\mathrm{B}}^{\mathrm{strong},1}=\frac{1}{2}J_2N+\frac{1}{3}J_1\sum_{i=1}^{N}(\vec{S}_i'\cdot\vec{S}_i+\vec{S}_i\cdot\vec{S}_{i+1}') \tag{6}$$

with the renormalized spin of rung block $S_i'=3/2$, which depicts a spin-($\frac{3}{2}$,1) Heisenberg chain with a renormalized AFM coupling $\frac{1}{3}J_1$. In the next step of RG procedure Hamiltonian (6) is projected to a $S''=1/2$ FM Heisenberg chain,

$$\tilde{H}_{\mathrm{B}}^{\mathrm{strong},2}=\frac{1}{6}(3J_2-5J_1)N-\frac{10}{27}J_1\sum_{i=1}^{N}\vec{S}_i''\cdot\vec{S}_{i+1}'', \tag{7}$$

whose FM excitations imply that the magnon excitations of the original system from S_G to S_G-1 are gapless with a quadratic dispersion relation in low energies. The sublattice magnetization is obtained as $m_{\mathrm{S}}=-\frac{1}{3}$, $m_\tau=\frac{5}{18}$, and $m_\sigma=\frac{5}{9}$, giving the spontaneous magnetization per unit cell $m=\frac{1}{2}$.

In the weak-coupling limit ($|J_2|\ll J_1$), we perform the RG on the block spins $\vec{S}_i$ and $\vec{\tau}_i$ with the doublet of total spin 1/2. The effective Hamiltonian is

$$\tilde{H}_{\mathrm{B}}^{\mathrm{weak},1}=-NJ_1-\sum_{i=1}^{N}\left(\frac{4}{9}J_1\vec{S}_i'\cdot\vec{S}_{i+1}'+\frac{1}{3}J_2\vec{S}_i'\cdot\vec{\sigma}_i\right) \tag{8}$$

with the renormalized spin $S_i'=1/2$, which describes a spin-1/2 FM Heisenberg chain with $\sigma=1$ pendant spins coupled by the renormalized AFM interaction $-\frac{1}{3}J_2$. The spin-wave results show that the excitations that correspond to those from S_G to S_G-1 in the original system are also gapless with

$$\omega_k\sim\frac{2}{9}J_1k^2 \tag{9}$$

for $k\to 0$. In the two limits, it is observed from Eqs. (6) and (9) that the low-energy behaviors of the gapless excitation are both dominated by J_1.

C. $J_1<0$ and $J_2>0$

For the strong-coupling limit ($J_2\gg|J_1|$), because of the strong AFM J_2, $\vec{\sigma}_i$ and $\vec{\tau}_i$ are renormalized by the doublet with total spin 1/2. The effective Hamiltonian is given by

$$\tilde{H}_{\mathrm{C}}^{\mathrm{strong},1}=-NJ_2-\frac{1}{3}J_1\sum_{i=1}^{N}(\vec{S}_i'\cdot\vec{S}_i+\vec{S}_i\cdot\vec{S}_{i+1}') \tag{10}$$

with $S'=1/2$. Equation (10) describes a spin-($\frac{1}{2}$,1) Heisenberg chain coupled by the renormalized AFM interaction $-\frac{1}{3}J_1$. In the second step of RG, Hamiltonian (10) is projected to a $S''=1/2$ FM Heisenberg chain,

$$\tilde{H}_{\mathrm{C}}^{\mathrm{strong},2}=-\left(J_2-\frac{J_1}{3}\right)N+\frac{4}{27}J_1\sum_{i=1}^{N}\vec{S}_i''\cdot\vec{S}_{i+1}'', \tag{11}$$

which unveils the gapless excitations from S_G to S_G-1 of the original system. The sublattice magnetization is obtained as $m_{\mathrm{S}}=\frac{2}{3}$, $m_\tau=\frac{1}{18}$, and $m_\sigma=-\frac{2}{9}$, giving rise to the spontaneous magnetization per unit cell $m=\frac{1}{2}$.

In the weak-coupling limit ($J_2\ll|J_1|$), the spins $\vec{S}_i$ and $\vec{\tau}_i$ are taken as a block, and the multiplet with spin 3/2 are kept to truncate the block Hilbert space. The effective Hamiltonian is obtained as

$$\tilde{H}_{\mathrm{C}}^{\mathrm{weak},1}=\frac{1}{2}NJ_1+\sum_{i=1}^{N}\left(\frac{2}{9}J_1\vec{S}_i'\cdot\vec{S}_{i+1}'+\frac{1}{3}J_2\vec{S}_i'\cdot\vec{\sigma}_i\right), \tag{12}$$

which describes a spin-3/2 FM Heisenberg chain with antiferromagnetically coupled pendant spins σ_i. The spin-wave analysis indicates that the effective system has a FM gapless excitation with

$$\omega_k\sim-J_1k^2 \tag{13}$$

for $k\to 0$. Analogous to the above cases, the low-energy behavior of the gapless branch in the two limits are determined by J_1, which can be seen from Eqs. (10) and (13).

Based on the RSRG analyses, one may observe that the different cases have distinct low-energy effective Hamiltonians, and the magnon excitations from S_G to S_G-1 are always FM and gapless, being consistent with those of the spin-($\frac{1}{2}$,1) mixed-spin chain. The dispersion relations near $k=0$ are found to be dominated by J_1 in both strong and weak couplings. The low-energy effective Hamiltonians for cases (B) and (C) in the strong-coupling limit are analogous except the magnitude of spin, whose thermodynamic properties will be compared in Sec. V.

IV. LOW-LYING EXCITATIONS AND MAGNETIC PROPERTIES

In this section, the low-lying excitations and magnetic properties are explored by means of the LSW (Refs. 2 and 3) and DMRG.[20,21] During the DMRG calculations, the chain length is taken as $L=300$, and the Hilbert space is truncated to 240 most relevant states. Open boundary conditions are adopted and the truncation error is less than 10^{-8} in all calculations.

A. $J_1>0$ and $J_2>0$

The Holstein-Primakoff (HP) transformations are introduced as follows:

$$\sigma_i^z=s_1-a_i^\dagger a_i,$$

$$\sigma_i^+=\sqrt{2s_1-a_i^\dagger a_i}a_i,$$

$$\sigma_i^-=a_i^\dagger\sqrt{2s_1-a_i^\dagger a_i} \tag{14}$$

for the sublattice of $\vec{\sigma}_i$ spins with $s_1=1$, and

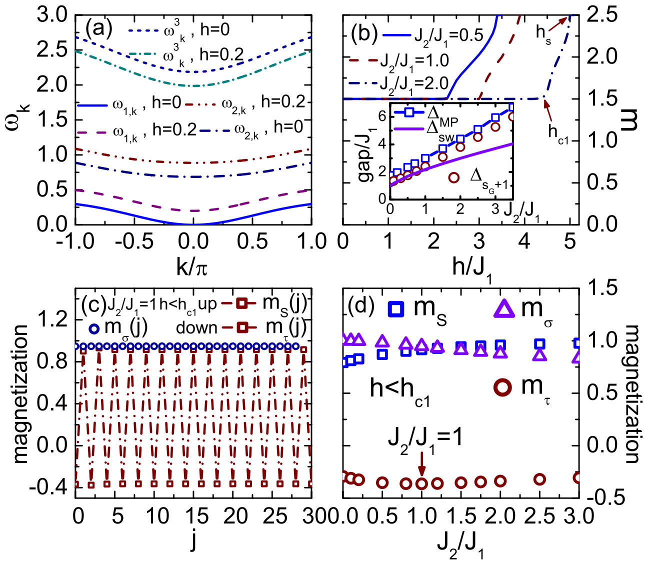

FIG. 2. (Color online) (a) Magnon excitation dispersion for case (a) with $J_1=J_2=1$ under different magnetic fields. (b) Magnetization curves for different J_2. The inset shows the coupling dependence of the gap Δ_{MP}, Δ_{SW}, and Δ_{S_G+1}. (c) Local magnetization as a function of lattice site for $h<h_{c1}$. (d) Coupling dependence of sublattice magnetization for $J_2/J_1=1$ and $h<h_c$.

$$\tau_i^z=-s_2+b_i^\dagger b_i,$$

$$\tau_i^+=b_i^\dagger\sqrt{2s_2-b_i^\dagger b_i},$$

$$\tau_i^-=\sqrt{2s_2-b_i^\dagger b_i}b_i \tag{15}$$

for the sublattice of spins $\vec{\tau}_i$ with $s_2=\frac{1}{2}$, where the operators a_i and b_i are bosons. The spins $\vec{S}_i$ are transformed in the similar way as Eq. (14) with bosonic operators c_i and $c_i^\dagger$. Thus, the magnon spectra can be obtained by diagonalizing the Hamiltonian after performing the Fourier and Bogoliubov transformations. As shown in Fig. 2(a), the magnon spectra consist of a gapless branch $\omega_{1,k}$ and two gapped ones $\omega_{2,k}$ and $\omega_{3,k}$. In the presence of a magnetic field h, both $\omega_{1,k}$ and $\omega_{2,k}$ increase, while $\omega_{3,k}$ decreases, indicating that $\omega_{1,k}$ and $\omega_{2,k}$ describe the magnons from S_G to S_G-1 while $\omega_{3,k}$ are those from S_G to S_G+1. For $J_2=0$, the spectra are reduced to a gapped and a gapless excitations, which agree exactly with those of the spin-$(\frac{1}{2},1)$ mixed-spin chain. When J_2 is set in, the gapless branch splits into $\omega_{1,k}$ and $\omega_{2,k}$. With increasing J_2, both $\omega_{2,k}$ and $\omega_{3,k}$ enhance. It is found that the low-energy dispersions near $k=0$ of the gapless branch $\omega_{1,k}$ are insensitive to J_2 but dominated by J_1 in a wide range of the coupling ratio, which covers the result obtained from the RSRG.

The magnetic curve $m(h)$ and low-energy gaps are then studied by the DMRG method. As shown in Fig. 2(b), $m(h)$ has a plateau at the spontaneous magnetization $m=\frac{3}{2}$, whose width Δ_{MP} increases with increasing J_2. In this figure, h_{c1} denotes the field where the plateau disappears, and h_s is the saturation field. For $J_2=0$, Δ_{MP} reduces to $1.759J_1$ of the spin-$(\frac{1}{2},1)$ mixed-spin chain, which is exactly the gap of its massive magnon branch.[10,11] The coupling dependence of Δ_{MP} is illustrated in the inset of Fig. 2(b), showing that Δ_{MP} increases almost as a linear behavior. The J_1 dependence of Δ_{MP} is also studied by taking J_2 as the energy scale, which is not presented here. It is found that Δ_{MP}/J_2 varies rather slowly with J_1, which means that Δ_{MP} is mainly scaled by J_2 in this case. The gap of the massive magnon branch $\omega_{3,k}$ (Δ_{SW}) is also shown in the inset of Fig. 2(b) in comparison to Δ_{MP}. The magnon gap obtained from the LSW appears to be smaller than Δ_{MP}, where the deviation increases for stronger J_2. It appears that the LSW underestimates the magnon gap from S_G to S_G+1.

We also compute the spin gap Δ_{S_G+1} from the ground state to the lowest state in the S_G+1 subspace, as shown in the inset of Fig. 2(b). Analogous to the spin-$(\frac{1}{2},1)$ mixed-spin chain, Δ_{S_G+1} is smaller than Δ_{MP}, indicating that Δ_{S_G+1} is also not a magnonlike excitation. But, it has a similar behavior with coupling to Δ_{MP}, which can thus be used to describe the low-energy behaviors. The spin gap from the ground state to the lowest state in the S_G-1 subspace is computed, which is found always vanishing and is consistent with the gapless branch $\omega_{1,k}$.

Next let us discuss the spin-spin correlation function and local magnetization in ground states. Figure 2(c) shows the local magnetization as a function of lattice site for $h<h_{c1}$. In the ground state, the spin-correlation functions along the chain have a long-range order and the spin fluctuations $\langle S_i^z S_j^z\rangle$-$\langle S_i^z\rangle\langle S_j^z\rangle$ decay rather rapidly (not presented here). Hence it is adequate to study only the local magnetization in the ground state. For $J_2=0$, it gives $m_\tau=-0.29248$ and $m_{\mathrm{S}}=0.79248$, exactly in agreement with the previous result.[2] After tuning on J_2, the coupling dependence of sublattice magnetization is shown in Fig. 2(d). The pendant spin magnetization m_σ is suppressed by the quantum fluctuations after tuning J_2, while m_{S} increases and approaches saturation for large J_2, confirming the results of the RSRG. The interesting phenomenon is the behavior of m_τ. As shown by the arrow in Fig. 2(d), m_τ decreases for $J_2/J_1<1$, and turns to increase when $J_2/J_1>1$, which has a turning point at $J_2/J_1=1$, as suggested by the result of the RSRG. Meanwhile, it can be seen that m_σ and m_{S} intersect near $J_2/J_1=1$. The changes in coupling dependence of the magnetic moments near $J_2/J_1=1$ may be owing to the competition of the two AFM interactions.

B. $J_1>0$ and $J_2<0$

To perform the LSW calculation, S_G and $\vec{\tau}_i$ spins are transformed as the form of Eq. (14) by the bosonic operators $(a_i,a_i^\dagger)$ and $(b_i,b_i^\dagger)$ with $s_1=1$ and $\frac{1}{2}$, respectively, while $\vec{S}_i$ are transformed as the form of Eq. (15) by $(c_i,c_i^\dagger)$ with $s_2=1$. As shown in Fig. 3(a), the spectra consist of a gapless and two gapped branches. In the presence of magnetic field, the gapless branch $\omega_{1,k}$ and the gapped branch $\omega_{3,k}$ increase, while the gapped branch $\omega_{2,k}$ decreases, indicating that $\omega_{1,k}$ and $\omega_{3,k}$ are the excitations from the sector S_G to S_G-1 while $\omega_{2,k}$ describes the excitations from S_G to S_G+1. It can be seen that the spectra in this case are quite different from those of case (A). The branch $\omega_{2,k}$ from S_G to S_G+1 is close

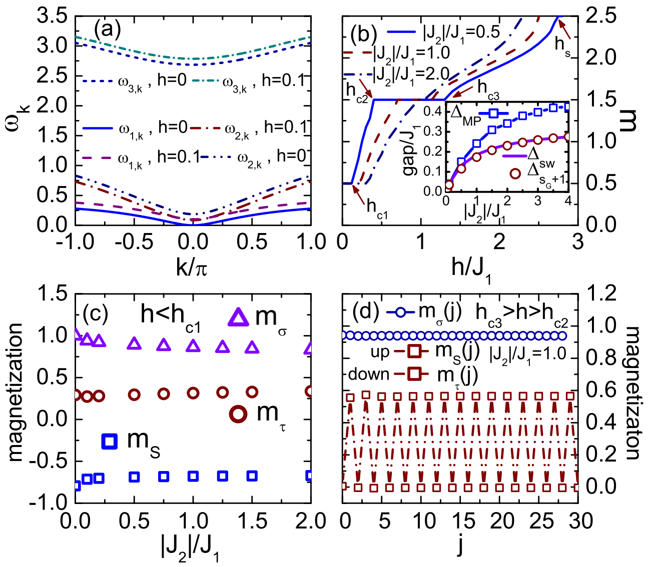

FIG. 3. (Color online) (a) Magnon excitation dispersion for case (b) with $J_1=1$ and $J_2=-1$. (b) Magnetization curves for different J_2. The inset shows the coupling dependence of the gap Δ_{MP}, Δ_{SW}, and Δ_{S_G+1}. (c) Coupling dependence of sublattice magnetization. (d) Local magnetization as a function of lattice site for $h_{c2}<h<h_{c3}$.

to the gapless branch $\omega_{1,k}$ for the present case, and with increasing $|J_2|$, it increases slightly. The resulting distinctions in the thermodynamics would be explored in Sec. V. With changing the couplings, it is found that the low-energy dispersions of the gapless branch $\omega_{1,k}$ near $k=0$ are dominated by J_1, which is consistent with the RSRG result.

The magnetic curve $m(h)$ and low-energy gaps are shown in Fig. 3(b). It can be seen that $m(h)$ exhibits two plateaus at $m=\frac{1}{2}$ and $\frac{3}{2}$. We denote the field where the $m=\frac{1}{2}$ plateau vanishes as h_{c1}, the lower and upper critical fields for the $m=\frac{3}{2}$ plateau as h_{c2} and h_{c3}, respectively, and h_s as the saturation field. With increasing $|J_2|$, the width of the $m=\frac{1}{2}$ plateau Δ_{MP} is enlarged slightly, while the $m=\frac{3}{2}$ plateau decreases and smears when $|J_2|/J_1 \gtrsim 2.0$. It should be noted that in some quasi-one-dimensional polymerized Heisenberg antiferromagnets, there might be a transition from the plateau state to the nonplateau state that is usually of the Kosterlitz-Thouless type.[22] Such a transition point cannot be numerically determined accurately owing to the finite-size length of the chain. Therefore, in the present case, whether a plateau-nonplateau transition with couplings at the $m=\frac{3}{2}$ plateau exists cannot be safely judged from our DMRG numerical results. The coupling dependence of Δ_{MP} is illustrated in the inset of Fig. 3(b), showing that Δ_{MP} increases with enhancing $|J_2|$, and different from case (A), Δ_{MP} goes to saturate at large $|J_2|$, which suggests that Δ_{MP} is mainly scaled by J_1 for large $|J_2|/J_1$. The coupling dependence of the magnon gap $\omega_{2,k=0}$ (Δ_{SW}) is also shown in the inset of Fig. 3(b). It can be seen that the spin wave is capable of describing the coupling dependence of magnon gap qualitatively, though it underestimates the value like in the case (A). The spin gap Δ_{S_G+1} from the ground state to the lowest state in the S_G+1 subspace is also computed. As shown in the inset of Fig. 3, Δ_{S_G+1} is less than Δ_{MP}, indicating that it is also not a magnonlike excitation, and its behavior for different coupling ratios is consistent with Δ_{MP} and Δ_{SW}.

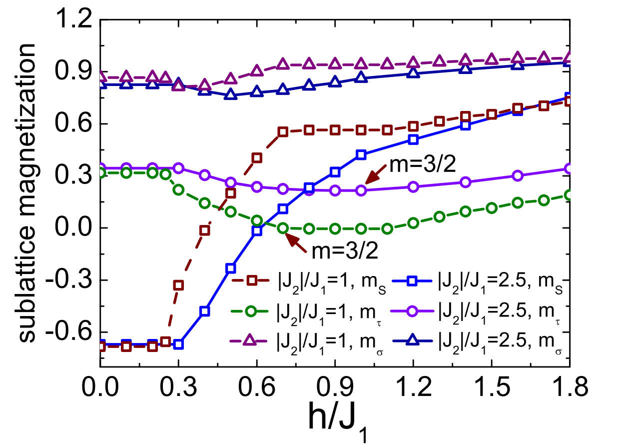

FIG. 4. (Color online) Magnetic field dependence of the sublattice magnetization m_{S}, m_τ, and m_σ for $|J_2|/J_1=1$ and 2.5. The arrows indicate the minimum of m_τ, where the magnetization per unit cell is $m=3/2$.

The coupling dependence of sublattice magnetization in the ground states is shown in Fig. 3(c). As the quantum fluctuations become strong after tuning J_2, the pendant spin magnetization m_σ decreases with increasing $|J_2|$, which is analogous to case (A). However, the FM coupling has different effects on the spins in the chain compared with the AFM J_2. With increasing $|J_2|$, both m_τ and m_{S} increase slightly, and m_τ does not show an extremum like in the case (A).

In the $m=\frac{3}{2}$ plateau region ($h_{c2}<h<h_{c3}$), the local magnetization is shown in Fig. 3(d) for $|J_2|/J_1=1$ as an example. It may be expected that all the local magnetic moments would increase from h_{c1} to h_{c2}. However, by comparing the local magnetization below h_{c1} [Fig. 3(c)] and in the plateau [Fig. 3(d)], it is surprising to notice that m_τ decreases from 0.3156 below h_{c1} to -0.0046 in h_{c2}. Therefore, the field dependence of sublattice magnetization is studied, as shown by m_{S}, m_τ, and m_σ for $|J_2|/J_1=1$ and 2.5 in Fig. 4. It can be seen that m_τ decreases continuously from h_{c1} to h_{c2} while m_σ decreases in a short range above h_{c1}. For a comparison, we also calculated the sublattice magnetization as a function of field for both the spin-$(\frac{1}{2},1)$ mixed-spin chain and the case (A). The results shows that the above behavior is not seen. Therefore, this decreasing behavior may be owing to the competition between the FM and AFM interactions in a magnetic field.

C. $J_1<0$ and $J_2>0$

For $J_1<0$ and $J_2>0$, the HP transformations are applied on the spins $\vec{S}_i$ and $\vec{\tau}_i$ with the form of Eq. (14) by $(b_i, b_i^\dagger)$ and $(c_i, c_i^\dagger)$ for $s_1=1$ and $\frac{1}{2}$, respectively, and that with the form of Eq. (15) is applied on $\vec{\sigma}_i$ for $s_2=1$ with $(a_i, a_i^\dagger)$. As shown in Fig. 5(a), the spectra consist of a gapless $(\omega_{1,k})$ and a gapped $(\omega_{3,k})$ magnon branches from the sector S_G to S_G-1, as well as a gapped one $(\omega_{2,k})$ from S_G to S_G+1, which can be identified by the shifts of the branches with the magnetic field. It is noticed that the gapped branch $\omega_{2,k}$ from S_G

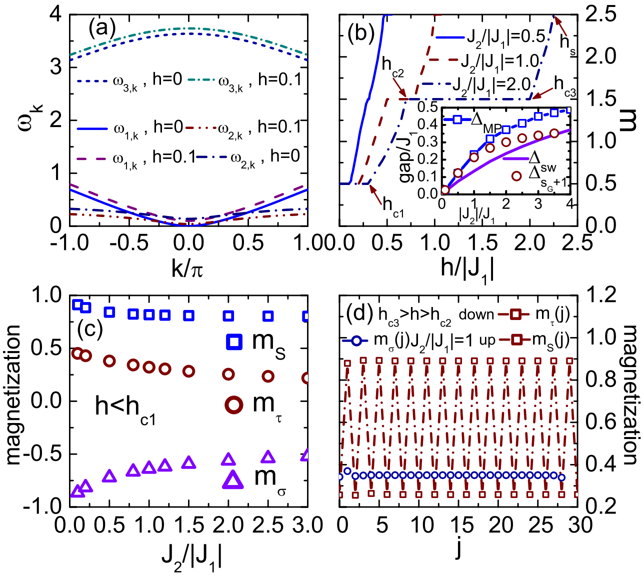

FIG. 5. (Color online) (a) Magnon excitation dispersion for case (c) with $J_1=-1$ and $J_2=1$. (b) Magnetization curves for different J_2. The inset shows the coupling dependence of the gap $\Delta_{\rm MP}$, $\Delta_{\rm SW}$, and Δ_{S_G+1}. (c) Coupling dependence of sublattice magnetization. (d) Local magnetization as a function of lattice site for $h_{c2}<h<h_{c3}$.

to S_G+1 is close to the gapless branch $\omega_{1,k}$, which is similar to the case (B), but $\omega_{2,k}$ has lower energies than $\omega_{1,k}$ for large wave momenta k in the present case. With increasing $J_2/|J_1|$, $\omega_{2,k}$ enhances and the intersected momenta of the two branches shift to higher values. A similar intersection of magnon branches has also been observed in the spin-$(\frac{1}{2},1)$ mixed-spin chain with AFM nearest-neighbor and FM next-nearest-neighbor interactions.[23] The influences of this intersection on the thermodynamics would be discussed in the next section. For $\omega_{1,k}$, it is found that the low-energy dispersions near $k=0$ are also dominated by J_1, which agrees with the RSRG analysis.

In Fig. 5(b), the magnetic curves $m(h)$ for different couplings are shown. Similar to case (B), $m(h)$ has two plateaux at $m=\frac{1}{2}$ and $\frac{3}{2}$, whose critical fields are denoted by the same symbols as the case (B). With increasing $J_2/|J_1|$, the width of the $m=\frac{1}{2}$ plateau ($\Delta_{\rm MP}$) extends, while that of the $m=\frac{3}{2}$ plateau is enlarged, which differs from the case (B) where the $m=\frac{3}{2}$ plateau decreases with increasing the coupling ratio. The inset of Fig. 5(b) shows the coupling dependence of the low-energy gaps $\Delta_{\rm MP}$, $\Delta_{\rm SW}$, and Δ_{S_G+1}. It can be seen that the gaps behave similarly to those in the case (B). The gaps approach to the saturation for large $J_2/|J_1|$, indicating that they are mainly scaled by J_1 in the large J_2 limit. The LSW also underestimates the magnon gap of $\omega_{2,k}$ as $\Delta_{\rm SW}$ is smaller than $\Delta_{\rm MP}$. Δ_{S_G+1} appears to be smaller than $\Delta_{\rm MP}$, which means that the spin gap from the ground state to the lowest state in the subspace with S_G+1 is also not a magnonlike excitation. In the ground states, the coupling dependence of the sublattice magnetization is displayed in Fig. 5(c). It can be seen that as the quantum fluctuations are induced by J_2, $m_{\rm S}$ and m_τ decrease with increasing J_2, while m_σ increases. In this case, the sublattice magnetic moments have more prominent variations with the change in the couplings than the previous cases.

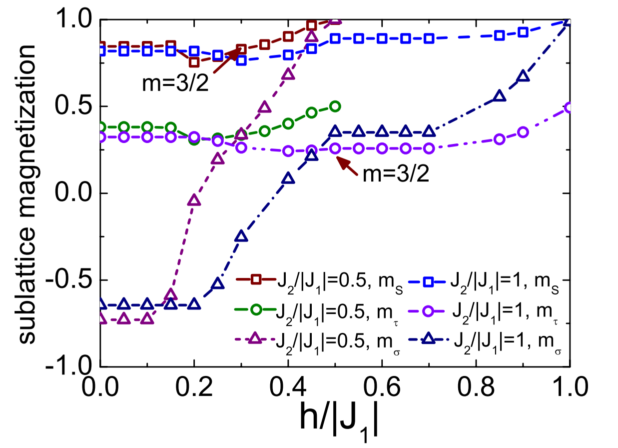

FIG. 6. (Color online) Magnetic field dependence of the sublattice magnetization $m_{\rm S}$, m_τ, and m_σ for $J_2/|J_1|=0.5$ and 1. The arrows indicate the magnetic field h_{c2}, where the magnetization per unit $m=3/2$.

In the $m=\frac{3}{2}$ plateau ($h_{c2}<h<h_{c3}$), the local magnetic moments for $J_2/|J_1|=1$ are shown in Fig. 5(d). By comparing the local magnetization below h_{c1} [Fig. 5(c)] and in the plateau [Fig. 5(d)], it is found that the decreasing feature of magnetization m_τ found in case (B) is also observed in the present case. The field dependence of sublattice magnetization is also studied. As illustrated in Fig. 6 for $J_2/|J_1|=0.5$ and 1.0, both m_τ and $m_{\rm S}$ have decreasing regions from h_{c1} to h_{c2}. Comparing with the sublattice magnetization of case (B), we notice that the two sublattice magnetizations that have a decreasing region from h_{c1} and h_{c2} are those coupled by FM interactions, and the decreasing behavior is only observed below the $m=\frac{3}{2}$ plateau.

V. TEMPERATURE DEPENDENCE OF SUSCEPTIBILITY AND SPECIFIC HEAT

From the above results, it can be seen that although the three cases entirely exhibit FI ground states, the low-lying excitations and magnetic properties are rather distinct. Thus, in this section, the temperature dependences of zero-field magnetic susceptibility and specific heat are explored by the TMRG method.[24] In the following calculations, the width of the imaginary time slice is taken as $\varepsilon=0.1$, and the error caused by the Trotter-Suzuki decomposition is less than 10^{-3}. During the TMRG iterations, 120 and 200 states are retained for the evaluation of the susceptibility and specific heat, respectively, and the temperature is down to $k_BT=0.025|J_1|$ in general. The truncation error is less than 10^{-4} in all calculations.

The temperature dependence of the susceptibility χ and susceptibility temperature product χT for the cases are shown in Figs. 7(a)–7(c). For case (A), the susceptibility, as shown in the inset of Fig. 7(a), diverges as $T\to 0$ due to the gapless branch $\omega_{1,k}$ [Fig. 2(a)]. Upon lowering temperature, χT decreases to a broad minimum at a temperature $T_{\min}$, and then increases to a peak at low temperature $T_{\rm peak}$. The minimum of χT is an indicative of the FI-like behavior similar to that in the spin-$(\frac{1}{2},1)$ mixed-spin chain. With increasing

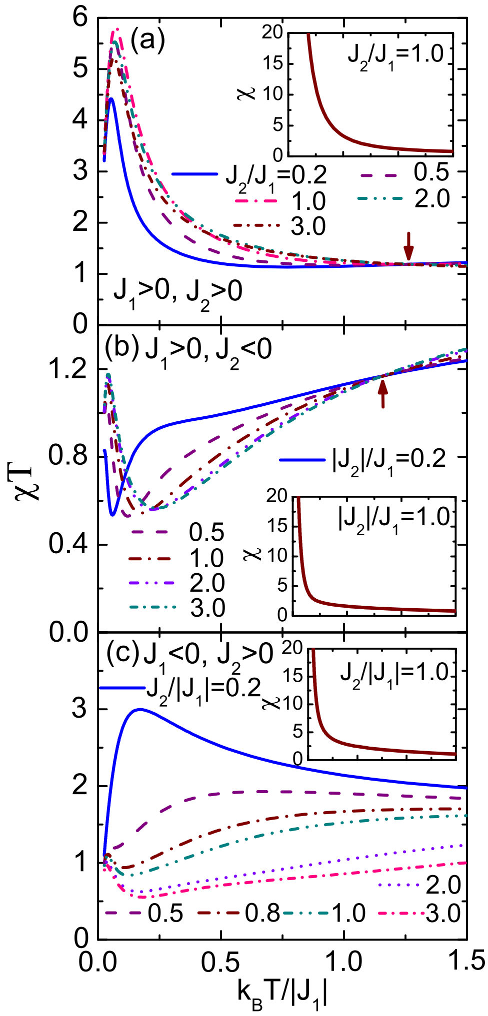

FIG. 7. (Color online) Temperature dependence of χT for (a) $J_1, J_2 > 0$; (b) $J_1 > 0$ and $J_2 < 0$; and (c) $J_1 < 0$ and $J_2 > 0$. The insets show the susceptibility as a function of temperature.

J_2/J_1, $T_{\rm min}$ shifts to higher temperatures, corresponding to the enhancement of the branches $\omega_{2,k}$ and $\omega_{3,k}$ with the increase in coupling ratios. Meanwhile, $\chi T_{\rm min}$ increases for $J_2/J_1 < 1$ and decreases for $J_2/J_1 > 1$. The maximum of $\chi T_{\rm min}$ is reached at $T_{\rm min} = 1.25 J_1$ when $J_2/J_1 = 1$. It is also noticed that the χT curves for different couplings intersect at the same temperature $1.25 J_1$, as shown by the arrow in Fig. 7(a). At low temperature, χT does not diverge, like that in the spin-$(\frac{1}{2}, 1)$ mixed-spin chain,[5] but has a sharp peak, which indicates that χ diverges equally or slower than $\frac{1}{T}$ as $T \to 0$.[25] For the low-temperature peak, it is unveiled that $T_{\rm peak}$ moves to higher temperatures with the increase in the height for $J_2/J_1 < 1$, while it approaches lower temperatures with the height decreasing for $J_2/J_1 > 1$. It can be seen that the finite-temperature magnetic properties have transition behaviors with the change in the couplings at $J_2/J_1 = 1$, which was also noted in the ground states in Sec. IV A.

For case (B), χ also goes to infinity as $T \to 0$ owing to the gapless branch $\omega_{1,k}$ [the inset of Fig. 7(b)]. As shown in Fig. 7(b), χT decreases rapidly to a minimum at $T_{\rm min}$ with decreasing temperature, and then increases to a peak at lower temperature, which is quite different from that in the case (A). With increasing $|J_2|/J_1$, both $T_{\rm min}$ and $\chi T_{\rm min}$ enhance. As indicated by the arrow in Fig. 7(b), χT curves for different couplings also intersect at a temperature $T \sim 1.15 J_1$. At low temperature, both the peak temperature and height of χT increase with increasing $|J_2|/J_1$. The peak suggests that χ diverges equally or slower than $\frac{1}{T}$ as $T \to 0$. Different from the case (A), the variation in χT in the present case with FM coupled pendants does not exhibit a transition behavior. It can be seen that J_2 has a great impact on the low-lying excitations as well as the magnetic properties at finite temperature.

Figure 7(c) illustrates the behaviors of χT for case (C). Although χ also diverges as $T \to 0$ [the inset of Fig. 7(c)], χT has rather distinct behaviors from cases (B) and (C) with $J_1 > 0$. For $J_2/|J_1| = 0.2$, χT increases to a broad maximum with decreasing temperature, and then declines. When $J_2/|J_1| > 0.5$, a minimum of χT emerges, and a small peak appears at a lower temperature. For $J_2/|J_1| > 1$, χT decreases to a minimum with declining temperature, showing the AFM feature, and then increases to a small peak, which is similar to that in the case (B). The minimum temperature $T_{\rm min}$ also increases with enhancing $J_2/|J_1|$. The convergence of χT as $T \to 0$ indicates that χ diverges equally or slower than $\frac{1}{T}$ as $T \to 0$ in this case. Compared with the above cases, no intersection of χT is observed for the present case with $J_1 < 0$. It should be noted that the similar behavior of χT has also been observed in the spin-$(\frac{1}{2}, 1)$ AFM chain with FM next-nearest-neighbor coupling,[23] which has an analogous low-lying excitations. As shown in Fig. 5(a), the gapped magnon branch $\omega_{2,k}$ has lower energies than the gapless branch $\omega_{1,k}$ for large wave momenta k. Thus, the low-lying excitations are dominated by $\omega_{2,k}$ for small J_2. With increasing $J_2/|J_1|$, $\omega_{2,k}$ enhances and $\omega_{1,k}$ gradually dominates the low-lying excitations. The branches $\omega_{1,k}$ and $\omega_{2,k}$ become analogous to that of the case (B) [Fig. 3(a)] for large $J_2/|J_1|$, yielding the behaviors of χT for $J_2/|J_1| > 1$ similar to that of the case (B) [Fig. 7(b)].

In Figs. 8(a)–8(c), the temperature dependences of the specific heat for the three cases are shown explicitly. For case (A), the specific heat has a prominent double-peak structure. When $J_2/J_1 = 0.5$, the high-temperature peak of specific heat is close to the peak temperature of that in the spin-$(\frac{1}{2}, 1)$ mixed-spin chain. With further increasing J_2, the low-temperature peak shifts to higher temperatures when $J_2/J_1 < 1$, while it keeps nearly intact for $J_2/J_1 > 1$. Meanwhile, the high-temperature peak continuously moves to higher temperatures, which might be owing to the enhancement of the gapped branch $\omega_{2,k}$ and $\omega_{3,k}$.

The temperature dependence of specific heat for case (B) is shown in Fig. 8(b). When $|J_2|/J_1 = 0.5$, the specific heat has double peaks, and the high-temperature peak is also close to the peak temperature of that in the spin-$(\frac{1}{2}, 1)$ mixed-spin chain. Compared with the specific heat of the case (A) with $J_2/J_1 = 0.5$ [Fig. 8(a)], it can be seen that the high-temperature behaviors above the high-temperature peak of the two cases agree well with each other, but the low-temperature behaviors are distinct. With increasing $|J_2|/J_1$ for $|J_2|/J_1 < 1$, the low-temperature peak moves to higher-

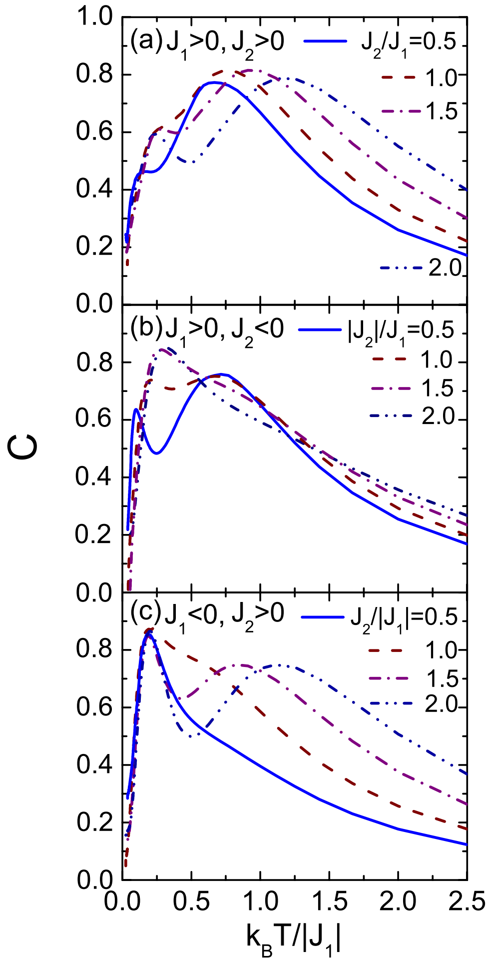

FIG. 8. (Color online) Temperature dependence of the specific heat C for (a) $J_1, J_2>0$; (b) $J_1>0$ and $J_2<0$; and (c) $J_1<0$ and $J_2>0$.

temperature side, while the high-temperature peak keeps nearly intact. For $|J_2|/J_1>1$, the double peaks merge into a single peak, which moves to higher temperatures slightly with increasing $|J_2|/J_1$. Analogous to χT, J_2 has also an essential effect on the behaviors of specific heat.

For case (C), the specific heat behaves quite differently from the above cases. For $J_2/|J_1|=0.5$, the specific heat shows a single peak instead of double peaks at low temperature. With increasing J_2 below $J_2/|J_1|=1$, the specific heat below the peak temperature keeps nearly unchanged, while the part above the peak temperature decreases more slowly, as shown in Fig. 8(c). For $J_2/|J_1|>1$, a high-temperature peak emerges, which moves to higher temperatures with increasing $J_2/|J_1|$. Meanwhile, the behaviors of specific heat below the low-temperature peak still retains nearly intact. The low-temperature peak seems to be insensitive to J_2 and is dominated by J_1.

For a comparison, we also calculated the thermal quantities by the LSW theory, which give rise to the similar behaviors for the three different cases. The results show that χT diverges as $T\to 0$ and the specific heat always exhibits double peaks. Although the obtained low-lying excitations are helpful to understand the thermodynamics, the quantitative results obtained from the LSW are not so good, which are thus not presented here.

VI. SUMMARY AND DISCUSSION

In this paper, the low-lying, magnetic and thermodynamic properties of the spin-$(\frac{1}{2},1)$ decorated mixed-spin chain with spin-1 pendant spins are systematically studied for three cases: (A) $J_1, J_2>0$; (B) $J_1>0$ and $J_2<0$; and (C) $J_1<0$ and $J_2>0$ by jointly using a few different methods. By means of the RSRG analysis, the low-energy effective Hamiltonians for each case in strong and weak couplings are obtained. It is found that although the effective Hamiltonians are different for three cases, their magnon excitations from S_G to S_G-1 are all FM and gapless, which agree with that of the spin-$(\frac{1}{2},1)$ mixed-spin chain without pendants. The low-energy dispersions of the gapless branch near $k=0$ are dominated by J_1 for each case, which is confirmed by the LSW results.

The low-lying excitations and magnetic properties are then investigated by the LSW and DMRG methods, respectively. The magnon spectra are found to consist of a gapless and a gapped branches from S_G to S_G-1, as well as a gapped branch from S_G to S_G+1, which have different features for three cases. For case (C), two low-energy branches have an unusual intersection. In a magnetic field, case (A) has a $m=\frac{3}{2}$ plateau, while both cases (B) and (C) exhibit two plateaux at $m=\frac{1}{2}$ and $\frac{3}{2}$. The low-energy gap of case (A) increases almost linearly with increasing the coupling ratio, while those of cases (B) and (C) increase and go to saturation for large $|J_2|$, which implies that the low-energy gap of the case (A) is mainly scaled by J_2, and those of the cases (B) and (C) are scaled by J_1 for large $|J_2|$. The sublattice magnetization of the spins coupled by FM interactions for cases (B) and (C) are found to decrease in some regions from h_{c1} to h_{c2} with the increase in the magnetic field, which may be attributed to the competition of the AFM and FM interactions in a magnetic field.

The zero-field thermodynamics are also explored by means of the TMRG method. It is unveiled that although χ diverges as $T\to 0$, χT has rather different behaviors for each cases. For case (A), χT has a broad minimum and a peak at low temperature. The curves of χT for different couplings intersect at a common temperature $1.25J_1$ and χT has a transition behavior with the couplings at $J_2/J_1=1$. For case (B), χT has a narrow minimum and a sharp peak at low temperature. The curves of χT for different couplings also intersect at a common temperature but χT never show a crossing behavior. For case (C), χT has a broad peak for $J_2/|J_1|<1$, and exhibits a broad minimum and a peak for $J_2/|J_1|>1$, showing two distinct features with changing the couplings due to the intersection of two low-lying excitations. Compared with the spin-$(\frac{1}{2},1)$ mixed-spin chain, there is a common feature for the three cases that χT converges as $T\to 0$, which implies that χ diverges equally or slower than $\frac{1}{T}$ as $T\to 0$.

The specific heat for case (A) has double peaks. For case (B), the specific heat has double peaks when $|J_2|/J_1<1$, which merge into a single peak as $|J_2|/J_1>1$. For case (C), however, the specific heat has a single peak when $J_2/|J_1|$

<1, while double peaks emerge when $J_2/|J_1|>1$. In a wide range of the coupling for case (C), the low-temperature peak appears to be insensitive to J_2, which mainly affects the high-temperature behaviors of the specific heat.

Based on the above results, it can be seen that the case (A) of the present system preserves some features of the spin-$(\frac{1}{2},1)$ mixed-spin chain, while the cases (B) and (C) exhibit more exotic properties that have not been observed in the mixed-spin chains. We expect that the magnetic and thermodynamic properties presented in this paper could be tested experimentally in future to unveil the effects induced by the pendant spins in the mixed-spin chains.

ACKNOWLEDGMENTS

We are grateful to Hui-Zhong Kou for helpful discussions. The work is supported in part by the NSFC (Grants No. 10625419, No. 10934008, and No. 90922033), the MOST of China (Grant No. 2006CB601102) and the Chinese Academy of Sciences.

*Corresponding author; gsu@gucas.ac.cn

[1] O. Kahn, Struct. Bonding (Berlin) **68**, 89 (1987); O. Kahn, *Molecular Magnetism* (VCH, New York, 1993); O. Kahn, Y. Pei, M. Verdaguer, J. P. Renard, and J. Sletten, J. Am. Chem. Soc. **110**, 782 (1988); P. J. van Koningsbruggen, O. Kahn, K. Nakatani, Y. Pei, J. P. Renard, M. Drillon, and P. Leggol, Inorg. Chem. **29**, 3325 (1990).

[2] S. K. Pati, S. Ramasesha, and D. Sen, Phys. Rev. B **55**, 8894 (1997).

[3] N. B. Ivanov, Phys. Rev. B **57**, R14024 (1998).

[4] C. J. Wu, B. Chen, X. Dai, Y. Yu, and Z. B. Su, Phys. Rev. B **60**, 1057 (1999).

[5] S. Yamamoto, Phys. Rev. B **59**, 1024 (1999); **61**, R842 (2000).

[6] A. K. Kolezhuk, H.-J. Mikeska, and S. Yamamoto, Phys. Rev. B **55**, R3336 (1997).

[7] A. K. Kolezhuk, H.-J. Mikeska, K. Maisinger, and U. Schollwöck, Phys. Rev. B **59**, 13565 (1999).

[8] T. Sakai and S. Yamamoto, Phys. Rev. B **60**, 4053 (1999); T. Sakai and K. Okamoto, *ibid.* **65**, 214403 (2002).

[9] E. H. Lieb and D. Mattis, J. Math. Phys. **3**, 749 (1962).

[10] S. Yamamoto, S. Brehmer, and H.-J. Mikeska, Phys. Rev. B **57**, 13610 (1998).

[11] S. Yamamoto and T. Sakai, Phys. Rev. B **62**, 3795 (2000).

[12] S. Yamamoto and T. Fukui, Phys. Rev. B **57**, R14008 (1998); S. Yamamoto, T. Fukui, K. Maisinger, and U. Schollwöck, J. Phys.: Condens. Matter **10**, 11033 (1998).

[13] K. Maisinger, U. Schollwöck, S. Brehmer, H.-J. Mikeska, and S. Yamamoto, Phys. Rev. B **58**, R5908 (1998).

[14] T. Mallah, S. Thiebaut, M. Verdaguer, and P. Veillet, Science **262**, 1554 (1993); O. Sato, T. Lyoda, A. Fujishima, and K. Hashimoto, *ibid.* **272**, 704 (1996); H.-Z. Kou, S. Gao, J. Zhang, G.-H. Wen, G. Su, R.-K. Zhang, and X.-X. Zhang, J. Am. Chem. Soc. **123**, 11809 (2001); E. Colacio, J. M. Domnguez-Vera, F. Lloret, A. Rodríguez, and H. Stoeckli-Evans, Inorg. Chem. **42**, 6962 (2003).

[15] H. Oshio, O. Tamada, H. Onodera, T. Ito, T. Ikoma, and S. Tero-Kubota, Inorg. Chem. **38**, 5686 (1999); R. Lescouëzec, F. Lloret, M. Julve, J. Vaissermann, M. Verdaguer, R. Llusar, and S. Uriel, *ibid.* **40**, 2065 (2001); R. Lescouëzec, J. Vaissermann, F. Lloret, M. Julve, and M. Verdaguer, *ibid.* **41**, 5943 (2002); J. Y. Yang, M. P. Shores, J. J. Sokol, and J. R. Long, *ibid.* **42**, 1403 (2003); J. T. Culp, J. H. Park, M. W. Meisel, and D. R. Talham, *ibid.* **42**, 2842 (2003).

[16] Hui-Zhong Kou, Wei-Wei Ni, Xin Liang, Zhong-Hai Ni, and Ru-Ji Wang (unpublished).

[17] A. Langari and P. Thalmeier, Phys. Rev. B **74**, 024431 (2006); P. Thalmeier and A. Langari, *ibid.* **75**, 174426 (2007); S. Mahmoudian and A. Langari, *ibid.* **77**, 024420 (2008).

[18] J. Goldstone, A. Salam, and S. Weinberg, Phys. Rev. **127**, 965 (1962).

[19] K. G. Wilson, Rev. Mod. Phys. **47**, 773 (1975); M. A. Martin-Delgado, in *Strongly Correlated Magnetic and Superconducting Systems*, Lecture Notes in Physics Vol. 478, edited by G. Sierra and M. A. Martin-Delgado (Springer, Berlin, 1997), and references therein.

[20] S. R. White, Phys. Rev. Lett. **69**, 2863 (1992); Phys. Rev. B **48**, 10345 (1993); U. Schollwöck, Rev. Mod. Phys. **77**, 259 (2005).

[21] B. Gu, G. Su, and S. Gao, Phys. Rev. B **73**, 134427 (2006); B. Gu and G. Su, Phys. Rev. Lett. **97**, 089701 (2006); Phys. Rev. B **75**, 174437 (2007); S. S. Gong and G. Su, *ibid.* **78**, 104416 (2008); S. S. Gong, S. Gao, and G. Su, *ibid.* **80**, 014413 (2009); S. S. Gong and G. Su, Phys. Rev. A **80**, 012323 (2009); Y. Zhao, S. S. Gong, W. Li, and G. Su, Appl. Phys. Lett. **96**, 162503 (2010); W. Li, S. S. Gong, Y. Zhao, and G. Su, Phys. Rev. B **81**, 184427 (2010).

[22] K. Okamoto, Solid State Commun. **98**, 245 (1996); B. Gu, G. Su, and S. Gao, J. Phys.: Condens. Matter **17**, 6081 (2005).

[23] S. Mohakud, S. K. Pati, and S. Miyashita, Phys. Rev. B **76**, 014435 (2007).

[24] R. J. Bursill, T. Xiang, and G. A. Gehring, J. Phys.: Condens. Matter **8**, L583 (1996); X. Wang and T. Xiang, Phys. Rev. B **56**, 5061 (1997); T. Xiang and X. Wang, in *Density-Matrix Renormalization: A New Numerical Method in Physics*, edited by I. Peschel, X. Wang, M. Kaulke, and K. Hallberg (Springer, New York, 1999), pp. 149–172.

[25] In order to investigate the low-temperature behavior of χT, we have performed the TMRG calculations to lower temperatures. However, as χT decreases rather sharply as $T\rightarrow 0$, it is hard to determine exactly whether χT converges to zero or just to a finite small value.